State-selective charge transfer between He-like ions and He

J. P. M. Beijers, R. Hoekstra, and R. Morgenstern
Kernfysisch Versneller Instituut, University of Groningen, Zernikelaan 25, 9747 AA Groningen, The Netherlands
(Received 1 July 1993)

We report absolute, state-selective cross sections for single-electron capture by He-like ions (N^{5+}, O^{6+}, F^{7+}, Ne^{8+}) colliding on He which were determined by vuv photon-emission spectroscopy. The impact energy was varied between 0.05 and 2 keV amu^{-1}. The experimental data are compared with theoretical predictions based on the classical overbarrier model, the Landau-Zener model, and existing close-coupling calculations.

PACS number(s): 34.70.+e

I. INTRODUCTION

The process of single-electron capture (SEC) by multiply charged ions colliding on neutral gas atoms is best understood for (quasi-) one-electron systems. The basic mechanism of SEC, i.e., resonant transfer of the active electron to an excited state of the projectile ion, is elegantly described by simple (semi)classical models such as the classical overbarrier model [1] and the Landau-Zener model [2]. These models are easily used to estimate the relevant cross sections. Very accurate predictions of detailed state-selective cross sections have been obtained with elaborate close-coupling calculations for many different collision systems [3]. One of the present challenges in this field of study is to achieve the same level of understanding of charge transfer in (quasi-)two-electron systems, e.g., collisions between multiply charged ions and helium. Most of the work performed to date has focused on the two-electron channels including double-electron capture and transfer ionization [4]. Although much progress has been made, particularly in identifying the different capture mechanisms, the large number of open channels greatly complicates detailed theoretical treatments of these two-electron processes.

In the present paper we concentrate on the SEC channels of some quasi-two-electron collision systems. In particular, we used vuv photon emission spectroscopy to determine total and state-selective SEC cross sections for the dominant and semidominant n channels in collisions of the He-like ions N^{5+}, O^{6+}, F^{7+}, and Ne^{8+} with He. The collision energy was varied between 0.05 and 2 keV amu^{-1}. We also performed calculations of total and state-selective cross sections based on the classical overbarrier model and the Landau-Zener model in order to show the usefulness and limitations of these models. Our experimental data provide stringent tests for realistic calculations of SEC processes in the above-mentioned (quasi-)two-electron systems. Furthermore, the present data might also be relevant for the plasma fusion community in relation to impurity diagnostics and control in the next generation of large tokamaks [5].

Several other groups have also studied SEC in the collision systems investigated here. These groups include Iwai *et al.* [6] and Justiniano *et al.* [7], who have determined total SEC cross sections using charge-state-analysis techniques. State-selective SEC cross sections for the O^{6+} + He system were measured by Liu *et al.* [8] using vuv photon emission spectroscopy, but at much higher impact energies (2–105 keV amu^{-1}) than in the present investigation. Finally, Waggoner *et al.* [9] measured the angular distributions of the scattered projectiles at specific impact energies. These distributions are very sensitive to the detailed dynamics of the charge transfer process (i.e., shape and participation of the relevant potential-energy curves; see also Cocke *et al.* [10]).

The present work is part of an ongoing project to set up and evaluate a database of total and state-selective cross sections for various collision processes between low-Z multiply charged ions and atomic hydrogen and helium. Previous related work by our group can be found in Refs. [11–14].

II. EXPERIMENT

We used a crossed beam apparatus to collide multiply charged ions with an effusive helium beam. The primary ion beam is extracted from an electron cyclotron resonance (ECR) ion source at a potential of 4 kV, transported to the collision chamber and, before being crossed with the target beam, decelerated with an electrostatic lens system to the desired collision energy. The target pressure at the scattering center is kept low enough to ensure single-collision conditions. vuv photons emitted by the product ions are detected with a grazing incidence monochromator (10–80 nm). A position sensitive detector enables simultaneous detection of lines within a range of about 20 nm. The monochromator is placed under the magic angle relative to the ion-beam axis and tilted by 45° in order to cancel all polarization-dependent effects. Two pairs of Helmholtz coils surrounding the collision chamber reduce the magnetic field perpendicular to the ion beam to less than a few μT. Our measurements are put on an absolute scale by normalizing to well-known cross sections of various ion and electron impact excitation processes. Details of the experimental setup and

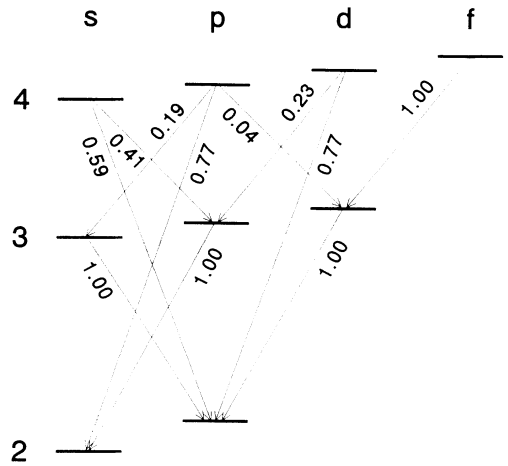

FIG. 1. Energy level diagram and allowed dipole transitions for a lithiumlike ion. The numbers along the lines represent the branching ratios for NV and OVI ions. These and other spectroscopic data relevant for the data analysis are listed in Table I.

calibration procedure can be found in Refs. [15,16].

In the collision systems investigated here SEC processes dominantly populate either the $n = 3$ shell (N^{5+}, O^{6+} + He) or the $n = 4$ shell (F^{7+}, Ne^{8+} + He) of the product ions. The relevant part of the energy level diagram of these ions is shown in Fig. 1 and typical spectra of the emitted vuv radiation are shown in Fig. 2. The N^{5+} and O^{6+} spectra are of much higher quality than the F^{7+} and Ne^{8+} spectra. The reason for this is that the former spectra were acquired with significantly higher projectile beam currents and higher detection efficiencies (because of the shorter wavelengths) than the latter ones. We determined the peak areas of the various lines by fitting Gaussian peak shapes with known widths and positions to the spectra. The vuv wavelengths and branching ratios used in the analysis are obtained from Ref. [17] and listed in Table I. Emission cross sections $\sigma_{\rm em}(nl \rightarrow mk)$ for the various transitions are determined from the corresponding peak areas $S(\lambda)$ with the relation

$$\sigma_{\rm em}(nl \rightarrow mk) = \frac{4\pi}{\omega}\frac{q}{K(\lambda)Q}\frac{S(\lambda)}{NL}\ , \qquad (1)$$

where λ is the wavelength of the $nl \rightarrow mk$ transition, ω the solid angle of observation, q the charge state of the projectile ions, Q the accumulated ion charge, $K(\lambda)$ the quantum yield of the detection system, N the effective target density, and L the observation length. Lifetime corrections are not necessary since all the product ions decay within view of the monochromator. The accumulated ion charge Q in Eq. (1) is corrected for the small fraction of metastables ($\approx 5\%$) present in the He-like projectile beams [18].

The state-selective cross sections $\sigma(nl)$ follow from the emission cross sections $\sigma_{\rm em}(nl \rightarrow mk)$ via

$$\sigma(nl) = \frac{\sigma_{\rm em}(nl \rightarrow mk)}{\beta_{nl,mk}} - \sum_{i\ (>n)} \sigma_{\rm em}(ik \rightarrow nl)\ , \qquad (2)$$

with $k = l + 1, l - 1$ and $\beta_{nl,mk}$ the branching ratio for the $nl \rightarrow mk$ transition (Table I). The second term in Eq. (2) accounts for cascade contributions from higher populated states.

Finally, the uncertainty in the present measurements is determined by counting errors and target density fluctuations (statistical uncertainties) and by the sensitivity calibration of the vuv monochromator (systematic uncertainty). The systematic uncertainty is estimated to be 20% and is independent of the collision energies studied here. A detailed error discussion relevant to the present experiment can be found in Ref. [16].

III. RESULTS

All results are displayed as a function of the impact energy in Figs. 3–7, together with other available experimental and theoretical data. The latter are represented by smooth curves and will be discussed in the following section. The error bars displayed in the figures represent one standard deviation of the statistical uncertainties. Figures 3 and 4 show the state-selective cross sections for capture into the dominant $n = 3$ shell for the N^{5+} + He and O^{6+} + He systems, respectively. Cascade contributions from the $n = 4$ shell to the various $3l$ substate populations are negligible for the N^{5+} + He system and small ($< 5\%$) for the O^{6+} + He system. The O^{6+} + He

TABLE I. vuv wavelengths λ and branching ratios β of the observed transitions in the indicated product ions (taken from Ref. [17]).

	$N^{4+\star}$		$O^{5+\star}$		$F^{6+\star}$		$Ne^{7+\star}$	
Transition	λ (nm)	β	λ (nm)	β	λ (nm)	β	λ (nm)	β
$3s$-$2p$	26.63	1.00	18.40	1.00	13.48	1.00	10.3	1.00
$3d$-$2p$	24.76	1.00	17.30	1.00	12.77	1.00	9.82	1.00
$3p$-$2s$	20.93	1.00	15.01	1.00	11.30	1.00	8.81	1.00
$4s$-$2p$	19.02	0.59	13.23	0.59	9.73	0.59	7.46	0.59
$4d$-$2p$	18.61	0.77	12.98	0.77	9.57	0.76	7.35	0.76
$4p$-$2s$	16.26	0.77	11.58	0.77	8.68	0.76	6.74	0.76
$4s$-$3p$					39.22	0.41	29.89	0.41
$4p$-$3d$					38.90	0.04	29.71	0.04
$4f$-$3d$					38.18	1.00	29.24	1.00
$4d$-$3p$					36.77	0.24	28.24	0.24
$4p$-$3s$					33.54	0.20	26.03	0.20

TABLE II. State-selective $[\sigma(3l)]$ and total $[\sigma(n = 3)]$ SEC cross sections with corresponding statistical errors (one standard deviation) in units of 10^{-16} cm^2 for N^{5+} + He collisions.

E (eV/amu)	$\sigma(3s)$	$\sigma(3p)$	$\sigma(3d)$	$\sigma(n = 3)$
1433	9.3 ± 0.7	3.22 ± 0.24	1.90 ± 0.16	14.4 ± 0.7
1129	9.6 ± 0.7	2.88 ± 0.24	1.71 ± 0.18	14.2 ± 0.8
879	11.7 ± 0.9	3.05 ± 0.25	1.59 ± 0.17	16.3 ± 0.9
661	12.0 ± 0.9	3.08 ± 0.25	1.36 ± 0.15	16.4 ± 1.0
461	12.5 ± 1.0	3.67 ± 0.31	1.29 ± 0.19	17.4 ± 1.0
363	13.4 ± 1.0	4.17 ± 0.33	1.28 ± 0.14	18.8 ± 1.1
254	14.1 ± 1.1	4.48 ± 0.35	1.12 ± 0.13	19.7 ± 1.1
192	13.8 ± 1.6	4.73 ± 0.54	0.86 ± 0.12	19.4 ± 1.7
161	15.9 ± 1.8	5.35 ± 0.61	1.31 ± 0.17	22.5 ± 1.9
123	15.6 ± 2.5	5.59 ± 0.89	0.99 ± 0.17	22.1 ± 2.6
92	14.2 ± 2.3	5.42 ± 0.86	0.84 ± 0.15	20.4 ± 2.4
67	12.3 ± 2.0	4.90 ± 0.78	0.77 ± 0.14	18.0 ± 2.1
49	10.8 ± 1.7	4.29 ± 0.70	0.81 ± 0.16	15.9 ± 1.9

data have been published previously [12], but are reproduced here for the sake of completeness. Figure 4 also shows the experimental data of Liu *et al.* [8], which they normalized to the data of Dijkkamp *et al.* [11] at 4.5 keV amu^{-1}. State-selective SEC cross sections for the $n = 4$ shells of the F^{7+} + He and Ne^{8+} + He systems are shown in Figs. 5 and 6, respectively. The small $3l$ cross sections for these collision systems have large uncertainties because of the $4l' \rightarrow 3l$ cascade corrections and are given only in tabular form. For the $\sigma(3s)$ and

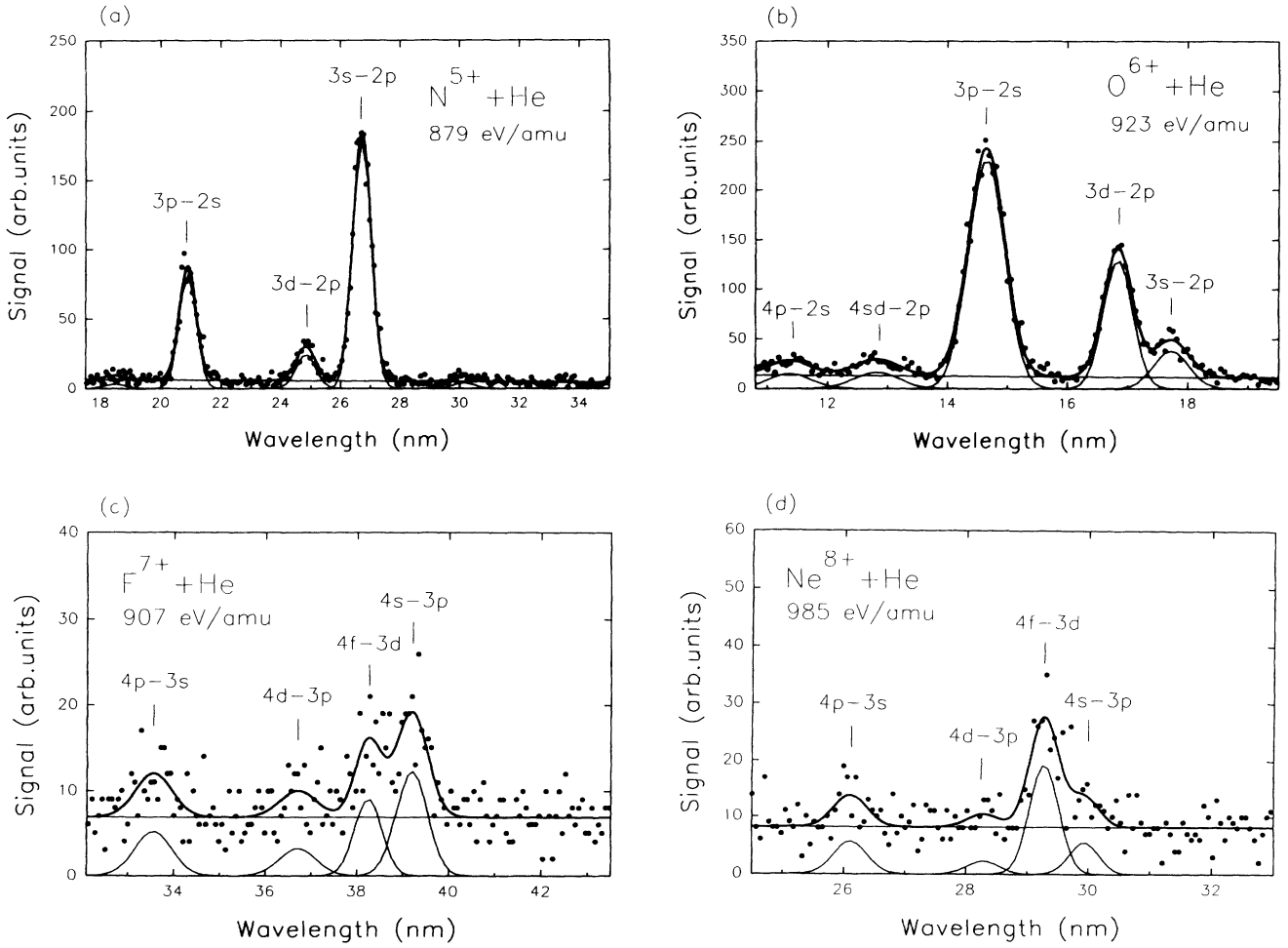

FIG. 2. Typical vuv emission spectra of (a) NV, (b) OVI, (c) FVII, and (d) NeVIII ions observed in charge-transfer collisions with He.

TABLE III. State-selective $[\sigma(3l)]$ and total $[\sigma(n = 3)]$ SEC cross sections with corresponding statistical errors (one standard deviation) in units of 10^{-16} cm^2 for O^{6+} + He collisions.

E (eV/amu)	$\sigma(3s)$	$\sigma(3p)$	$\sigma(3d)$	$\sigma(n = 3)$
1505	1.53 ± 0.15	6.69 ± 0.47	3.11 ± 0.24	11.3 ± 0.6
1186	1.23 ± 0.15	6.66 ± 0.47	3.13 ± 0.24	11.0 ± 0.6
923	1.02 ± 0.12	5.93 ± 0.48	3.19 ± 0.29	10.1 ± 0.6
695	0.86 ± 0.10	5.34 ± 0.43	2.93 ± 0.27	9.12 ± 0.52
484	0.57 ± 0.09	4.89 ± 0.40	3.08 ± 0.28	8.54 ± 0.50
380	0.52 ± 0.08	4.32 ± 0.35	3.21 ± 0.29	8.05 ± 0.46
267	0.37 ± 0.08	3.55 ± 0.29	3.31 ± 0.30	7.23 ± 0.43
215	0.20 ± 0.07	2.86 ± 0.40	2.62 ± 0.35	5.69 ± 0.54
169	0.24 ± 0.08	2.90 ± 0.40	3.24 ± 0.40	6.39 ± 0.57
136	0.14 ± 0.08	1.83 ± 0.35	2.52 ± 0.45	4.49 ± 0.58
110	0.10 ± 0.07	1.48 ± 0.30	2.43 ± 0.45	4.01 ± 0.55
85	0.20 ± 0.10	1.65 ± 0.33	2.61 ± 0.50	4.46 ± 0.60
62	0.15 ± 0.08	1.07 ± 0.22	2.81 ± 0.53	4.02 ± 0.58

$\sigma(3p)$ capture cross sections of the Ne^{8+} + He system we could only determine an upper bound of 5×10^{-17} cm^2. Finally, total cross sections for SEC into the $n = 3$ or $n = 3 + 4$ states for the investigated collision systems are shown in Fig. 7. The data of Iwai *et al.* [6] and Justiniano *et al.* [7] represent total $q \rightarrow q - 1$ charge transfer cross sections including contributions from transfer ionization and capture into n levels other than the ones indicated. This could account for the differences between our total cross sections and those given by Iwai *et al.* [6]; see, for example, Fig. 7(c). All present experimental data are given numerically in the Tables II–VI, together with their statistical uncertainties.

The experimental data show that the magnitudes and energy dependences of the state-selective SEC cross sections are strongly specific for each collision system. In

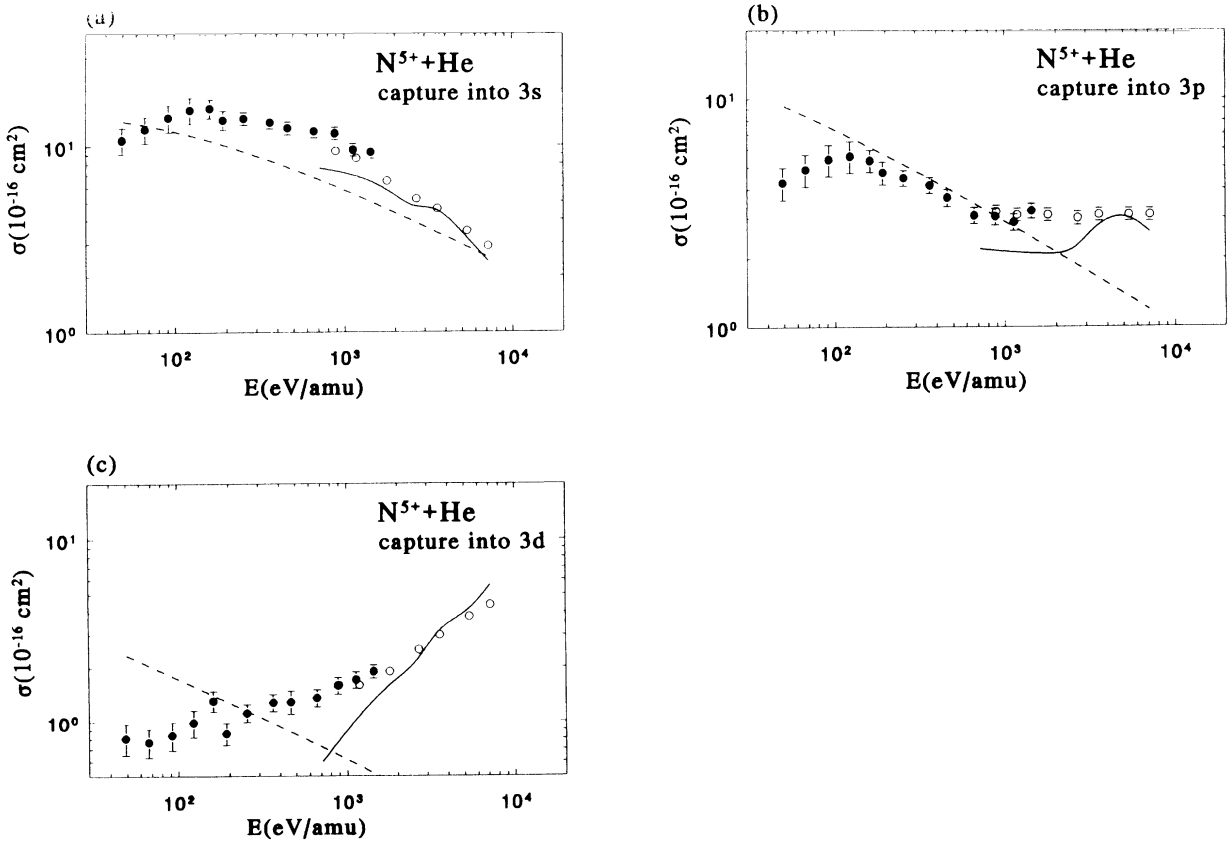

FIG. 3. State-selective cross sections for single-electron capture into the $n = 3$ shell of N^{4+} in N^{5+} + He collisions. The error bars represent one standard deviation of the statistical uncertainty. The systematic uncertainty is estimated to be 20%. Experiment: •, this work; ○, Dijkkkamp *et al.* [11]. Theory: ——, (MO) Bacchus-Montabonel [25]; - - -, (LZ) see Eq. (13).

TABLE IV. State-selective $[\sigma(3l)]$ and total $[\sigma(n = 3)]$ SEC cross sections with corresponding statistical errors (one standard deviation) in units of 10^{-16} cm^2 for F^{7+} + He collisions.

E (eV/amu)	$\sigma(3s)$	$\sigma(3p)$	$\sigma(3d)$	$\sigma(n = 3)$
1478	0.42 ± 0.10	0.80 ± 0.25	0.94 ± 0.40	2.16 ± 0.48
1165	0.36 ± 0.12	0.33 ± 0.26	0.63 ± 0.40	1.32 ± 0.49
907	0.28 ± 0.10	0.58 ± 0.27	0.54 ± 0.38	1.40 ± 0.48
682	≤ 0.20	0.23 ± 0.23	≤ 0.55	0.47 ± 0.49
373	0.11 ± 0.09	0.40 ± 0.33	≤ 0.55	0.69 ± 0.50
262	≤ 0.19	0.51 ± 0.55	≤ 0.67	0.88 ± 0.68
211	0.12 ± 0.12	0.79 ± 0.52	0.36 ± 0.36	1.27 ± 0.66
166	≤ 0.21	0.94 ± 0.59	0.39 ± 0.38	1.40 ± 0.72
133	≤ 0.17	0.66 ± 0.50	0.34 ± 0.34	1.05 ± 0.63
108	≤ 0.20	1.42 ± 0.74	≤ 0.46	1.57 ± 0.84
83	≤ 0.18	0.90 ± 0.73	≤ 0.49	1.02 ± 0.83

the next section we will try to understand the observed trends on the basis of the (semi)classical overbarrier and Landau-Zener models and compare the experimental data with existing quantum-mechanical close-coupling calculations.

IV. DISCUSSION

A. The classical overbarrier model

According to the classical overbarrier model SEC takes place when the Coulombic barrier, which separates the potential wells of the projectile and target nuclei, drops below the binding energy of the active electron with decreasing distance between the collision partners. This happens at an internuclear distance R_{CB}, which depends only on the charge q of the projectile ion and the ionization potential I_t of the target atom via (see [1] and references therein)

$$R_{CB} = \frac{2q^{\frac{1}{2}} + 1}{I_t} . \tag{3}$$

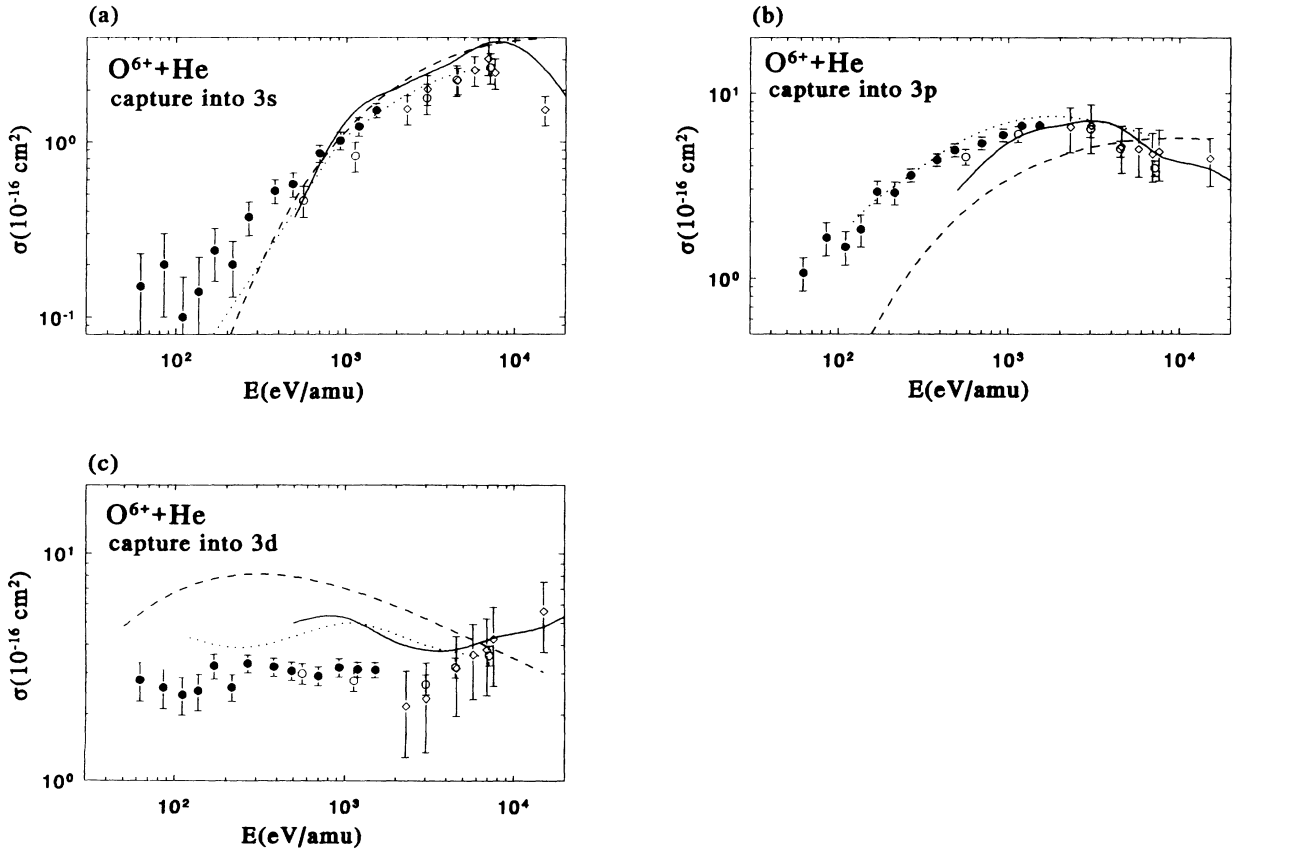

FIG. 4. State-selective cross sections for single-electron capture into the $n = 3$ shell of O^{5+} in O^{6+} + He collisions. Experiment: •, this work; ○, Dijkkamp *et al.* [11]; ◇, Liu *et al.* [8]. Theory: ——, (AO) Fritsch and Lin [26]; · · ·, (MO) Shimakura *et al.* [27]; – – –, (LZ) see Eq. (13).

TABLE V. State-selective $[\sigma(4l)]$ and total $[\sigma(n = 4)]$ SEC cross sections with corresponding statistical errors (one standard deviation) in units of 10^{-16} cm^2 for F^{7+} + He collisions.

E (eV/amu)	$\sigma(4s)$	$\sigma(4p)$	$\sigma(4d)$	$\sigma(4f)$	$\sigma(n = 4)$
1478	3.19 ± 0.59	2.50 ± 0.28	2.51 ± 0.50	3.00 ± 0.33	11.2 ± 0.9
1165	4.27 ± 0.75	2.10 ± 0.25	1.88 ± 0.64	2.13 ± 0.36	10.4 ± 1.1
907	5.01 ± 0.77	2.50 ± 0.24	1.93 ± 0.70	1.56 ± 0.28	11.0 ± 1.1
682	4.50 ± 0.80	2.25 ± 0.24	1.80 ± 0.70	2.06 ± 0.32	10.6 ± 1.1
475	6.06 ± 0.94	2.54 ± 0.25	2.23 ± 0.87	1.64 ± 0.32	12.5 ± 1.3
373	7.06 ± 0.92	2.30 ± 0.25	2.04 ± 0.70	0.94 ± 0.26	12.3 ± 1.2
262	7.2 ± 1.1	2.06 ± 0.29	1.42 ± 0.88	0.55 ± 0.23	11.2 ± 1.5
211	6.4 ± 1.0	2.37 ± 0.31	1.75 ± 0.80	0.45 ± 0.23	11.0 ± 1.3
166	7.4 ± 1.2	2.42 ± 0.31	1.98 ± 0.80	0.30 ± 0.21	12.1 ± 1.5
133	6.5 ± 1.4	2.45 ± 0.40	1.42 ± 0.80	≤ 0.3	10.4 ± 1.7
108	7.8 ± 1.5	3.14 ± 0.54	1.6 ± 1.0	≤ 0.2	12.5 ± 1.9
83	7.9 ± 1.5	2.60 ± 0.45	1.5 ± 1.0	≤ 0.2	12.0 ± 1.9

The total SEC cross section is taken to be proportional to the geometrical cross section

$$\sigma_t = A\pi R_{\mathrm{CB}}^2 , \tag{4}$$

with A the proportionality constant. The value $A = 0.5$ has been shown to give the best overall agreement for the present collision systems [11,19]. Assuming that the electron is transferred resonantly from the target to the projectile at the internuclear distance R_{CB}, its asymptotic binding energy I_q at the projectile ion is given by

$$I_q = I_t + \frac{q-1}{R_{\mathrm{CB}}} . \tag{5}$$

In the extended overbarrier model this binding energy I_q is smeared out into a so-called classical reaction window because of the finite time available for the charge transfer. The reaction window is assumed to be Gaussian with a width ΔE proportional to the square root of the im-

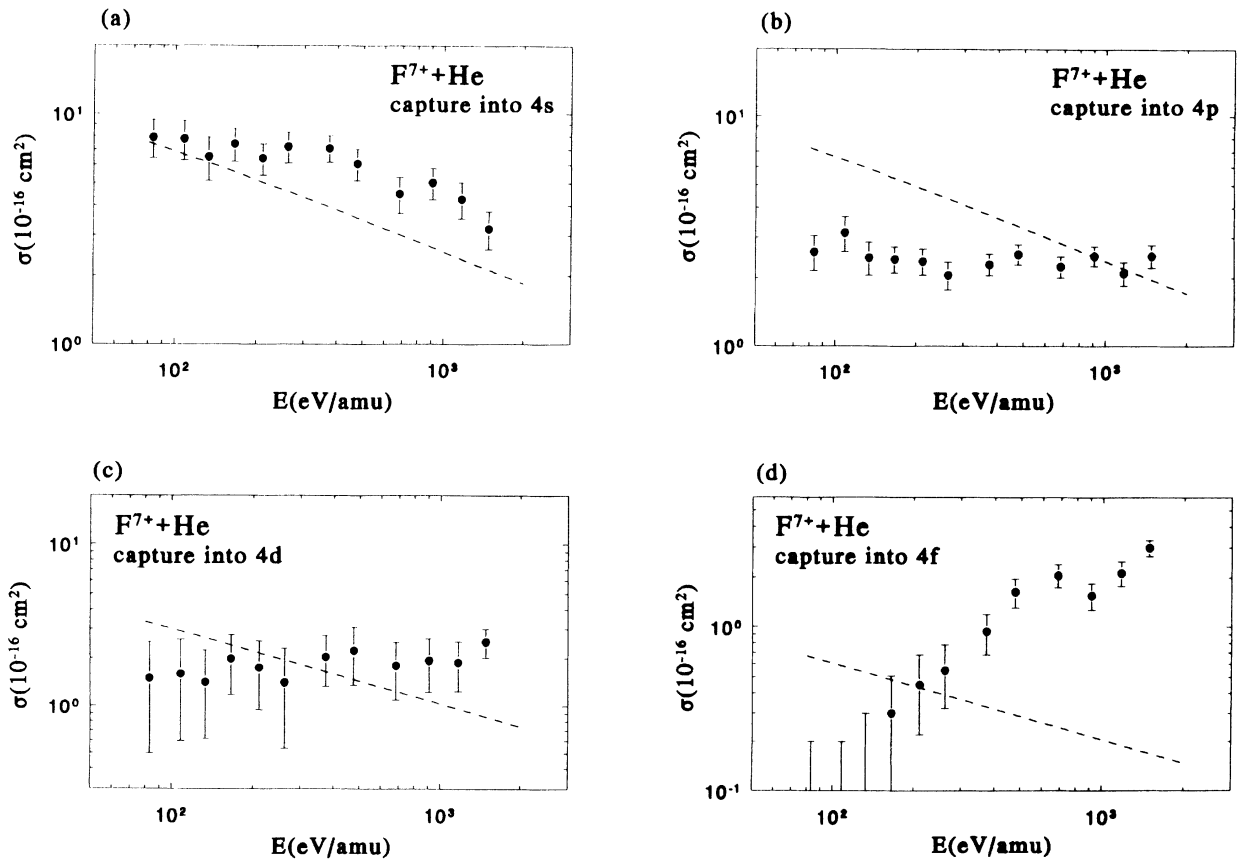

FIG. 5. State-selective cross sections for single-electron capture into the $n = 4$ shell of F^{6+} in F^{7+} + He collisions. See Fig. 3 for symbols.

TABLE VI. State-selective [$\sigma(3d)$ and $\sigma(4l)$] and total [$\sigma(n = 3+4)$] SEC cross sections with corresponding statistical errors (one standard deviation) in units of 10^{-16} cm^2 for Ne^{8+} + He collisions. The $3s$ and $3p$ capture cross sections are smaller than 5×10^{-17}cm^2.

E (eV/amu)	$\sigma(3d)$	$\sigma(4s)$	$\sigma(4p)$	$\sigma(4d)$	$\sigma(4f)$	$\sigma(n = 3+4)$
1605	1.5 ± 1.0	8.5 ± 2.0	9.9 ± 2.0	6.0 ± 2.0	6.5 ± 1.0	32.4 ± 3.7
1265	1.0 ± 1.0	8.6 ± 3.4	12.1 ± 1.5	5.3 ± 1.8	6.2 ± 1.2	33.2 ± 4.5
985	0.9 ± 0.9	7.3 ± 2.5	12.2 ± 3.8	7.9 ± 2.0	5.5 ± 0.9	33.8 ± 4.7
740	1.3 ± 0.9	7.0 ± 2.3	13.7 ± 2.8	7.0 ± 2.0	5.0 ± 1.0	34.0 ± 4.2
516	1.1 ± 0.7	4.6 ± 1.2	8.1 ± 2.2	4.1 ± 1.7	4.0 ± 1.0	21.9 ± 3.2
404	0.5 ± 0.5	4.0 ± 1.1	7.0 ± 1.5	3.2 ± 1.2	3.8 ± 0.8	18.7 ± 2.5
285	0.5 ± 0.5	3.5 ± 1.3	7.0 ± 1.5	2.4 ± 1.0	3.5 ± 0.8	16.9 ± 2.5
229	0.3 ± 0.3	2.7 ± 1.3	5.0 ± 2.0	2.6 ± 1.0	2.1 ± 0.4	12.7 ± 2.6

pact velocity v [1]. By examining the positions of the final projectile states with respect to the classical reaction window one can make qualitative predictions concerning the state-selective SEC cross sections on the basis of the overbarrier model.

We have done this for the present collision systems. The total SEC cross sections according to Eq. (4) are denoted in Fig. 7 by arrows and are in reasonable agreement with the experimental data. The O^{6+} + He system shows the largest discrepancies with the classical predictions, particularly at the lower impact energies. This can be understood from the reaction windows which are shown in Fig. 8. For the O^{6+} + He system none of the states are resonant with respect to the reaction window, while for N^{5+} + He the $3l$ states and for F^{7+}, Ne^{8+} + He the $4l$ states are all lying inside their respective reaction windows.

Apart from considerations based on the reaction window concept, this version of the classical overbarrier model cannot make quantitative predictions of state-selective SEC cross sections. However, in Refs. [20,21] it is shown that a simple extension of the classical overbarrier model enables one to calculate the distribution over the angular momentum substates of the dominantly

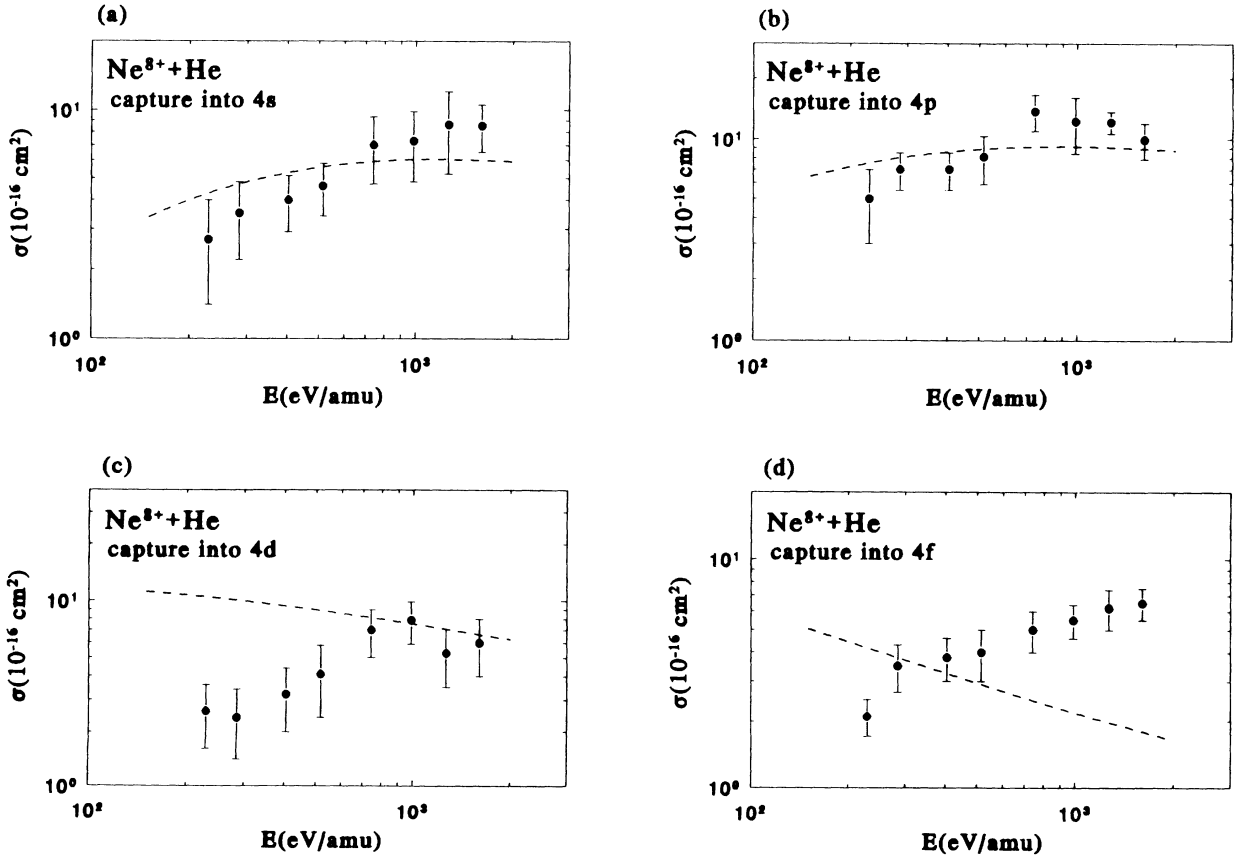

FIG. 6. State-selective cross sections for single-electron capture into the $n = 4$ shell of Ne^{7+} in Ne^{8+} + He collisions. See Fig. 3 for symbols.

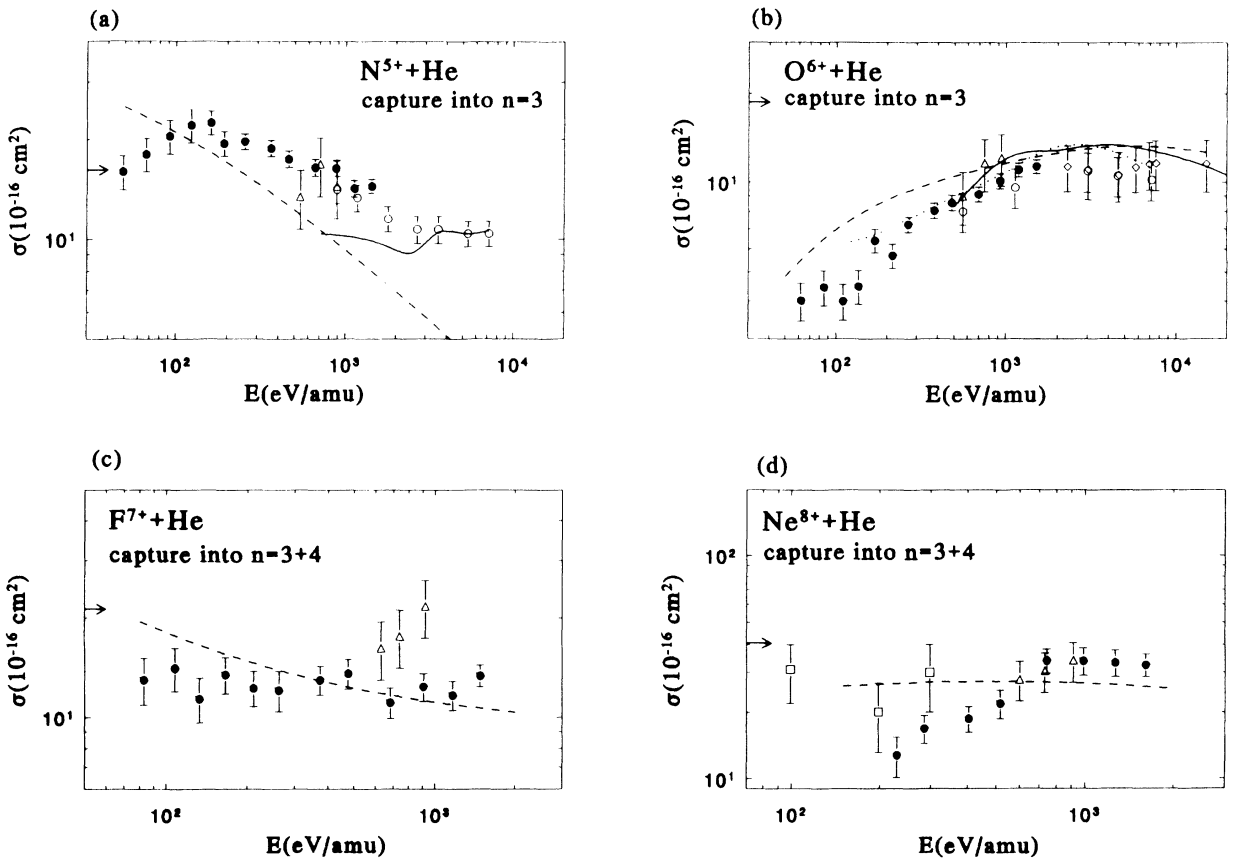

FIG. 7. Total SEC cross sections. See Figs. 3–6 for symbols; in addition: △, Iwai *et al.* [6]; □, Justiniano *et al.* [7].

populated n level in the product ions. The validity of the model was confirmed by comparison with a few illustrative examples (N^{5+}, O^{6+} + H, H_2). Here we will test the extended model with the present experimental data. The basic assumption is that the angular momentum L^* of the target electron as seen by the projectile ion, $L^* = b\,v$ with b the impact parameter and v the impact velocity, is conserved during the charge-transfer process. The angular momentum L^* is related to the angular momentum quantum number L via $L^* = L + \frac{1}{2}$. The total SEC cross

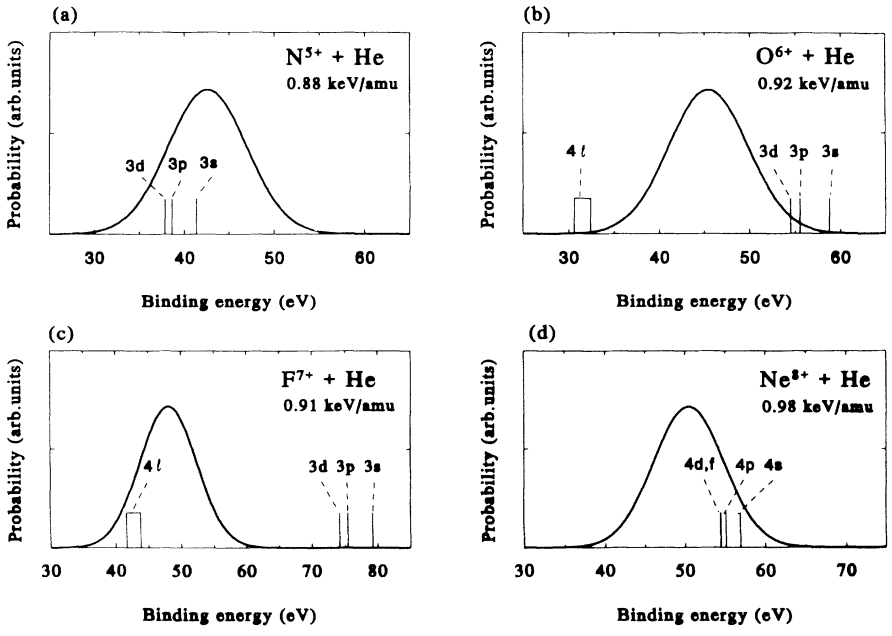

FIG. 8. Reaction windows for single-electron capture in collisions of (a) N^{5+}, (b) O^{6+}, (c) F^{7+}, and (d) Ne^{8+} with He. The positions of the relevant states of the product ions are indicated.

section σ_t can then be decomposed into concentric rings labeled by L, which correspond to the populated angular momentum substates of the projectile ion:

$$\sigma_L = A_L \, 2\pi \int_0^{R_{CB'}} W_L(b) \, b \, db \, . \tag{6}$$

The L-dependent proportionality constant A_L is given by [21]

$$A_L = \frac{2L+1}{2L+1+n_t^2} \, , \tag{7}$$

with n_t the principal quantum number of the active electron in the target atom. The upper integration limit $R_{CB'}$ in Eq. (6) depends not only on q and I_t (as in the original overbarrier model), but also on L [20]. The probability function $W_L(b)$ describes the conservation of the angular momentum L^* as discussed above. In Ref. [20] it is assumed that the active electron has a definite angular momentum $L^* = b\,v$, so that

$$W_L(b) = \Theta(L+1-bv)\,\Theta(bv-L) \, , \tag{8}$$

with Θ the Heaviside step function. On the other hand, the Gaussian reaction window causes the angular momentum L^* of the captured electron to be distributed around the value $b\,v$ with a Gaussian distribution function [21]. The probability function $W_L(b)$ then becomes

$$W_L(b) = \frac{1}{\sqrt{\pi}\Delta L}\left\{\exp\left[-\left(\frac{L^*-vb}{\Delta L}\right)^2\right] + \exp\left[-\left(\frac{L^*+vb}{\Delta L}\right)^2\right]\right\} . \tag{9}$$

The width ΔL of the L^* distribution is determined by the momentum distribution of the electrons when they cross the potential barrier and depends on the width ΔE of the reaction window [21].

Following Ref. [20] we have tested the extended classical model by comparing the expectation value of the angular momentum in the final state,

$$\langle L^* \rangle = \frac{\sum_{L=0}^{n-1}(L+\frac{1}{2})\sigma_L}{\sum_{L=0}^{n-1}\sigma_L} \, , \tag{10}$$

with our experimental results. For the experimental $\langle L^* \rangle$ the factor $(L+\frac{1}{2})$ in Eq. (10) is replaced by its exact quantal expression $\sqrt{L(L+1)}$. Figure 9 shows the experimental and theoretical results for $\langle L^* \rangle$ as a function of the impact velocity v for the various collision systems. The dashed curves are calculated using Eq. (8). The structure in these curves is caused by the opening of increasingly higher L channels with increasing impact velocity v. Allowing for a distribution of angular momenta according to Eq. (9) gives the dotted curves which do not show the L structure and generally fit the experimental data better than the dashed curves. However, large discrepancies between the experimental points and both models remain for the O^{6+} and Ne^{8+} + He systems. The main reason for this is that for these systems high L states are populated resulting in large $\langle L^* \rangle$ values even at small impact velocities. This agrees with the energetic positions of the high L states within their respective reaction windows as shown in Fig. 8 and is therefore simply

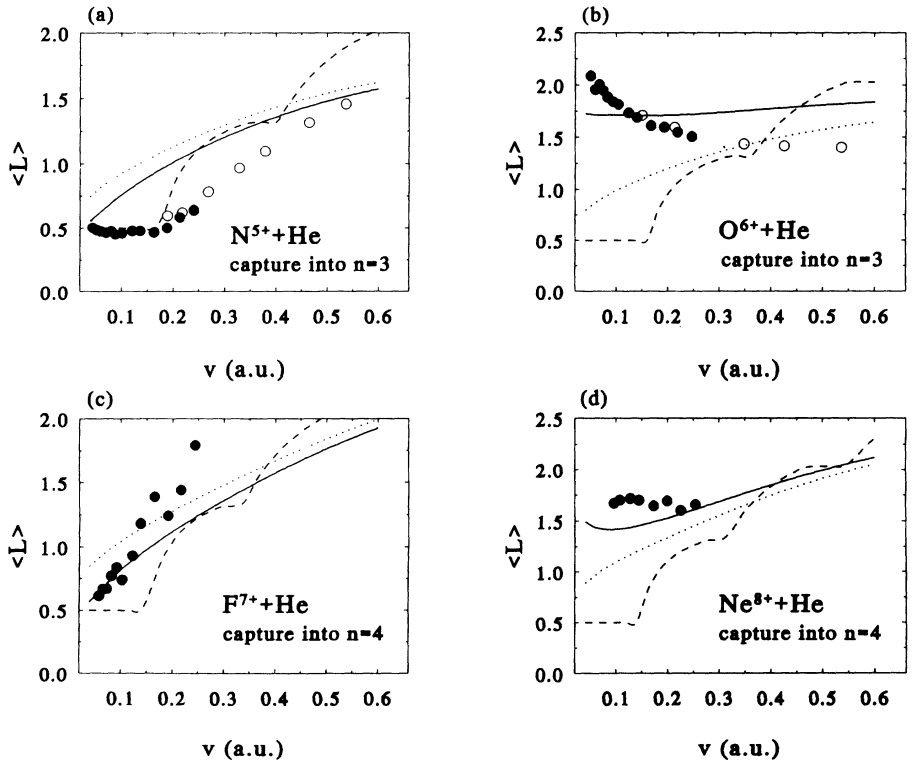

FIG. 9. Average angular momentum $\langle L^* \rangle$ as a function of the projectile velocity v in (a) $N^{4+}(n=3)$, (b) $O^{5+}(n=3)$, (c) $F^{6+}(n=4)$, and (d) $Ne^{7+}(n=4)$ following SEC collisions with He. Experiment: same as in Fig. 3. Theory: - - - , using definite angular momenta L^* according to Eq. (8); $\cdots$, using an angular momentum distribution according to Eq. (9); —— , using Gaussian multiplication factor as explained in the text.

accounted for by multiplying Eq. (6) with the Gaussian factor $\exp[-(\frac{E_{nL}-I_q}{\Delta E})^2]$. This procedure results in the solid curves of Fig. 9 which clearly show better agreement with the experimental data points for the O^{6+}, Ne^{8+} + He systems and at the same time does not spoil the good agreement for the N^{5+}, F^{7+} + He systems.

To summarize, the present experimental data once again confirm that the classical overbarrier model correctly describes the main mechanism of the SEC process. Simple formulas enable one to predict total SEC cross sections generally within a factor of 2. A straightforward extension of the classical overbarrier model as described in Refs. [20,21] predicts angular momentum distributions which agree fairly well with the experimental data. However, quantum-mechanical models must be used in order to understand detailed state-selective SEC cross sections.

B. The Landau-Zener model

We have used the multichannel Landau-Zener model to calculate the state-selective SEC cross sections relevant for the present collision systems. The application of this model to SEC transitions in collisions between multiply charged ions and neutrals is reviewed in Ref. [22]. The Landau-Zener model is valid in the adiabatic velocity regime where the nuclear motion is governed by suitable potential-energy curves. In this model electronic transitions occur at avoided crossings between adiabatic potential-energy curves and are induced by radial couplings only. Transitions which are induced by rotational couplings are neglected in the standard Landau-Zener model.

The probability for a transition from an ingoing adiabatic potential-energy curve 1 to an outgoing curve 2 is $2p(1-p)$ with the probability p for a single traverse of the crossing given by [22]

$$p = \exp\left(\frac{-2\pi H_{12}^2}{\Delta F v_{\rm rad}}\right) . \qquad (11)$$

Here the transition matrix element H_{12} is one half of the splitting of the adiabatic potential-energy curves at the crossing point R_C, ΔF the difference in slopes of the corresponding diabatic curves at R_C, and $v_{\rm rad}$ the radial velocity at R_C. The crossing point R_C is calculated by assuming an ion-induced dipole interaction for the ingoing curve 1 and a repulsive Coulomb interaction for the outgoing curve 2. For H_{12} we use the Olson-Salop-Taulbjerg (OST) form

$$H_{12}^{\rm OST} = (9.13 f_{nl}/\sqrt{q}) \exp(-1.324 R_C\, \alpha/\sqrt{q}) , \qquad (12)$$

with the factor f_{nl} allowing for capture into the nl state of partly stripped ions and $\alpha = \sqrt{2\, I_t}$ [2]. The OST matrix element is based on an empirical fit to exact calculations of the adiabatic potential-energy curves [23]. The state-selective cross section for capture into the nl state of the product ion which correlates asymptotically with the outgoing potential-energy curve 2 is then given by

$$\sigma(nl) = 2\pi \int_0^{R_C} 2p(1-p)\, b\, db . \qquad (13)$$

Generalization of Eq. (13) to N states is straightforward, see, for example, Ref. [24].

The results of our multichannel Landau-Zener calculations are shown as the dashed curves in Figs. 3–7. All $3l$ and $4l$ substates have been taken into account. As a general rule one can observe that the s substates are reproduced very well, but discrepancies occur for the higher l states. In particular, while the experimental $3d$ (N^{5+}) or $4f$ (F^{7+}, Ne^{8+}) SEC cross sections clearly increase with increasing impact energy the Landau-Zener predictions show exactly the opposite trend. This is probably caused by the neglect of rotational coupling in the Landau-Zener model. Thus it appears that this coupling is not very important for capture into the lower l states, but becomes more important for the higher l states of the dominantly populated n shell. Apart from this limitation the Landau-Zener model gives reasonable estimates of total and state-selective SEC cross sections for the present collision systems, particularly considering the minimal amount of numerical work involved.

C. Close-coupling models

Close-coupling models presently constitute the most sophisticated quantum-mechanical calculations of SEC transitions in slow collisions between multiply charged ions and neutrals [3]. These models are based on a numerical solution of the complete electronic Hamiltonian using atomic (AO's) or molecular orbitals (MO's) as basis functions. Most of the calculations have been performed on (quasi-) one-electron systems, but some work has been done on the N^{5+} and O^{6+} + He collision systems.

In Ref. [25] a MO calculation is presented for the N^{5+} + He system, which is shown as a solid line in Figs. 3 and 7(a). The calculation reproduces the experimental data very well for impact energies larger than 3 keV amu^{-1}, but underestimates the data for smaller impact energies. This is also evident from the total SEC cross section shown in Fig. 7(a). Notice, however, that the trend in the $3d$ cross section is reproduced by the MO calculation as opposed to the Landau-Zener model. For the O^{6+} + He system both AO and MO close-coupling calculations have been performed [26,27]. These are shown as solid and dotted lines in Figs. 4 and 7(b), respectively. The AO and MO calculations generally reproduce the experimental data fairly well, but both models overestimate the $3d$ cross section throughout the entire energy region. Plotting the relative cross sections shows that while both AO and MO models reproduce the experimental data for the $3s$ state very well, for the $3p$ and $3d$ states the MO model agrees better with the experimental data in the low-energy region and the AO model is better in the high-energy region [12].

V. CONCLUSIONS

In this paper we have studied single-electron capture in collisions of the He-like ions N^{5+}, O^{6+}, F^{7+}, and Ne^{8+} with He in the impact energy range between 0.05 and 2 keV amu^{-1} using photon emission spectroscopy. From the observed spectra absolute, state-selective cross sections were determined for the dominantly populated nl states.

The experimental data were compared with different theoretical models. The most simple model is the classical overbarrier model which presents a classical description of the main mechanism responsible for SEC. With this model total SEC cross sections are generally reproduced within a factor of 2. A straightforward extension of the classical model incorporating angular momentum effects is in fair agreement with the observed angular momentum distributions of the dominantly populated n-shell. We have proposed a slight modification of this extended model to also take the classical reaction window into account.

The state-selective nl cross sections were compared with a semiclassical Landau-Zener model and quantum-mechanical AO and MO close-coupling models. For the Landau-Zener model we used Olson-Salop-Taulbjerg transition matrix elements. The Landau-Zener model reproduces the s substates fairly well, but particularly for the highest l states severe discrepancies can occur. This is attributed to the neglect in the Landau-Zener model of the rotational interaction which mostly affect the populations of the higher l states. Finally, the N^{5+} and O^{6+} data were compared with existing AO and MO close-coupling calculations. Although these state-of-the-art models do resolve the shortcomings of the Landau-Zener model and generally reproduce the experimental data, there is still room for improvement particularly for the lower impact energies.

ACKNOWLEDGMENTS

We wish to thank J. Eilander and J. Sijbring for their excellent technical support. This work is part of the research program of the Stichting voor Fundamenteel Onderzoek der Materie with financial support from the Stichting voor Nederlands Wetenschappelijk Onderzoek.

[1] A. Niehaus, J. Phys. B **19**, 2925 (1986).
[2] K. Taulbjerg, J. Phys. B **19**, L367 (1986).
[3] W. Fritsch and C. D. Lin, Phys. Rep. **202**, 1 (1991).
[4] M. Barat and P. Roncin, J. Phys. B **25**, 2205 (1992).
[5] R. K. Janev, Comment At. Mol. Phys. **26**, 83 (1991).
[6] T. Iwai, Y. Kaneko, M. Kimura, N. Kobayashi, S. Ohtani, K. Okuno, S. Takagi, H. Tawara, and S. Tsurubuchi, Phys. Rev. A **26**, 105 (1982).
[7] E. Justiniano, C. L. Cocke, T. J. Gray, R. Dubois, C. Can, W. Waggoner, R. Schuch, H. Schmidt-Böcking, and H. Ingwersen, Phys. Rev. A **29**, 1088 (1984).
[8] C. J. Liu, R. W. Dunford, H. G. Berry, R. C. Pardo, K. O. Groeneveld, M. Hass, and M. L. A. Raphaelian, J. Phys. B **22**, 1217 (1989).
[9] W. Waggoner, C. L. Cocke, L. N. Tunnell, C. C. Havener, F. W. Meyer, and R. A. Phaneuf, Phys. Rev. A **37**, 2386 (1988).
[10] C. L. Cocke, E. Y. Kamber, L. N. Tunnell, S. L. Varghese, and W. Waggoner, Nucl. Instrum. Methods A **262**, 89 (1987).
[11] D. Dijkkamp, Yu S. Gordeev, A. Brazuk, A. G. Drentje, and F. J. de Heer, J. Phys. B **18**, 737 (1985).
[12] J. P. M. Beijers, R. Hoekstra, A. R. Schlatmann, R. Morgenstern, and F. J. de Heer, J. Phys. B **25**, 463 (1992).
[13] J. P. M. Beijers, R. Hoekstra, R. Morgenstern, and F. J. de Heer, J. Phys. B **25**, 4851 (1992).
[14] R. Hoekstra, J. P. M. Beijers, F. J. de Heer, and R. Morgenstern, Z. Phys. D **25**, 209 (1993).
[15] R. Hoekstra, Ph. D. thesis, University of Groningen, 1990 (unpublished).
[16] R. Hoekstra, J. P. M. Beijers, A. R. Schlatmann, R. Morgenstern, and F. J. de Heer, Phys. Rev. A **41**, 4800 (1990).
[17] A. Lindgard and S. E. Nielsen, At. Data Nucl. Data Tables **19**, 533 (1977).
[18] M. Mack, Nucl. Instrum. Methods B **23**, 74 (1987).
[19] H. Ryufuku, K. Sasaki, and T. Watanabe, Phys. Rev. A **21**, 745 (1980).
[20] J. Burgdörfer, R. Morgenstern, and A. Niehaus, J. Phys. B **19**, L507 (1986).
[21] J. Burgdörfer, R. Morgenstern, and A. Niehaus, Nucl. Instrum. Methods B **23**, 120 (1987).
[22] R. K. Janev and Hannspeter Winter, Phys. Rep. **117**, 265 (1985).
[23] R. E. Olson and A. Salop, Phys. Rev. A **14**, 579 (1976).
[24] R. K. Janev, D. S. Belić, and B. H. Bransden, Phys. Rev. A **28**, 1293 (1983).
[25] M. Bacchus-Montabonel, Phys. Rev. A **40**, 6088 (1989).
[26] W. Fritsch and C. D. Lin, J. Phys. B **19**, 2683 (1986).
[27] N. Shimakura, H. Sato, M. Kimura, and T. Watanabe, J. Phys. B **20**, 1801 (1987).